Journal of Applied Physics

Alloy segregation at stacking faults in zincblende GaN heterostructures

Cite as: J. Appl. Phys. **128**, 145703 (2020); https://doi.org/10.1063/5.0015157
Submitted: 26 May 2020 . Accepted: 21 September 2020 . Published Online: 14 October 2020

B. Ding, M. Frentrup, S. M. Fairclough, M. J. Kappers, M. Jain, A. Kovács, D. J. Wallis, and R. A. Oliver

Journal of Applied Physics ARTICLE scitation.org/journal/jap

Alloy segregation at stacking faults in zincblende GaN heterostructures

Cite as: J. Appl. Phys. **128**, 145703 (2020); doi: 10.1063/5.0015157
Submitted: 26 May 2020 · Accepted: 21 September 2020 ·
Published Online: 14 October 2020

View Online Export Citation CrossMark

B. Ding,[1,a)] M. Frentrup,[1] S. M. Fairclough,[1] M. J. Kappers,[1] M. Jain,[2] A. Kovács,[3] D. J. Wallis,[1,2,4] and R. A. Oliver[1,a)]

AFFILIATIONS

[1]Department of Materials Science and Metallurgy, University of Cambridge, 27 Charles Babbage Road, Cambridge CB3 0FS, United Kingdom
[2]Kubos Semiconductors Ltd, Future Business Centre, Kings Hedges Road, Cambridge CB4 2HY, United Kingdom
[3]Ernst Ruska-Centre for Microscopy and Spectroscopy with Electrons, Forschungszentrum Jülich, Jülich 52425, Germany
[4]Centre for High Frequency Engineering, University of Cardiff, Queen's Building, Cardiff CF24 3AA, United Kingdom

[a)]**Authors to whom correspondence should be addressed:** bd371@cam.ac.uk and rao28@cam.ac.uk

ABSTRACT

Current cubic zincblende III-Nitride epilayers grown on 3C-SiC/Si(001) substrates by metal-organic vapor-phase epitaxy contain a high density of stacking faults lying on the {111} planes. A combination of high-resolution scanning transmission electron microscopy and energy dispersive x-ray spectrometry is used to investigate the effects of alloy segregation around stacking faults in a zincblende III-nitride light-emitting structure, incorporating InGaN quantum wells and an AlGaN electron blocking layer. It is found that in the vicinity of the stacking faults, the indium and aluminum contents were a factor of 2.3 ± 1.3 and 1.9 ± 0.5 higher, respectively, than that in the surrounding material. Indium and aluminum are also observed to segregate differently in relation to stacking faults with indium segregating adjacent to the stacking fault while aluminum segregates directly on the stacking fault.

I. INTRODUCTION

Despite the commercially successful rise of GaN-based optoelectronics over the last two decades, the so-called "green gap" problem[1] remains unsolved to date. The term refers to the sharp drop in quantum efficiency for InGaN-based emitters at longer wavelengths beyond the blue spectral range.[2] Approaching the green spectral range from the red side using arsenide and phosphide-based III-V compounds proves equally frustrating.[3,4] While the scientific debate on the origin of this efficiency problem in InGaN-based emitters is continuing, the focus is on factors affecting the radiative and nonradiative recombination processes, in particular, carrier localization at alloy fluctuations in InGaN alloys, the increase in lattice-mismatch induced strain, and reductions in material quality with the increasing InN fraction employed to reach longer wavelengths.[5–7]

A potential strategy to avoid such problems, which are related to intrinsic properties of wurtzite c-plane heterostructures, is the application of the nonpolar zincblende (zb) phase. Zincblende GaN-based structures in the (001) orientation are free from both spontaneous polarization and piezoelectric fields, have a smaller bandgap than the wurtzite (wz) phase, and are hence predicted to be more efficient green emitters.[8] With suitable substrates, zb-GaN epitaxial growth has been demonstrated by molecular beam epitaxy (MBE)[9–13] and metal-organic vapour-phase epitaxy (MOVPE).[14–18] As the zb phase is the thermodynamically metastable phase, the first challenge is to achieve phase purity, i.e., avoiding the formation of wz inclusions. Highly phase pure zb-GaN on 3C-SiC/(001) Si can be achieved by careful control of the growth conditions.[19–23] Nevertheless, {111} stacking faults (SFs) remain the most abundant planar defect in epitaxial layers, interrupting the ABCABCABC bi-layer stacking of the zb phase. An illustration of an intrinsic SF is shown in Fig. 1, where the stacking order is changed to ABC**AC**ABCA. While little is known about the role of SFs in zb-GaN, Kemper *et al.*[24] have reported that SFs are nonradiative centers. Furthermore, it has been proposed[25] that local electric

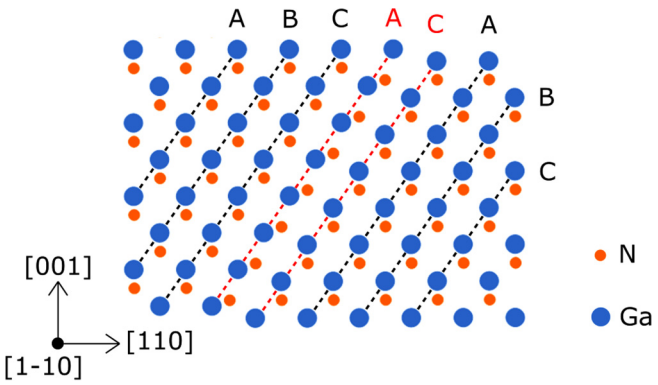

FIG. 1. A schematic diagram of a single intrinsic stacking fault, in which case a "-B-" bi-layer is missing. The faulty region is labeled by red letters.

fields may be formed across and between SFs as well as wz inclusions in zb-GaN. These fields may result in band bending, altering locally the bandgap. The impact of SFs on the ternary alloy composition in zb III-nitrides remains almost entirely unexplored. Here, using transmission electron microscopy techniques, we studied the In and Al segregation of SFs intersecting InGaN and AlGaN epilayers, respectively, incorporated into a zb-GaN-based light-emitting structure.

II. EXPERIMENTAL

The zb-GaN heterostructure was grown by MOVPE in a 6×2-in. Thomas Swan close-coupled showerhead reactor. The growth conditions used to achieve a high zb phase purity are described elsewhere.[23] Compared to wz-GaN growth, much lower temperatures (between 850 °C and 910 °C) and moderate V–III ratios (between 38 and 300) are required. The substrate used for the sample was a 20×20 mm^2 piece of a 150 mm diameter 3C-SiC/Si substrate (Anvil Semiconductors Ltd), consisting of a $\sim 3\,\mu$m thick 3C-SiC layer grown onto 1000 μm thick Si(001) with a 4° miscut toward the [110] in-plane direction. A schematic diagram of the zb-GaN light-emitting structure is shown in Fig. 2. Five InGaN quantum wells (QWs) of 3 nm thickness separated by 11 nm GaN barriers form the active region of the structure emitting at around 460 nm. The growth continued with 10 nm undoped GaN after the last barrier, followed by the growth of 15 nm Mg doped AlGaN, designed to function as an electron blocking layer. A 180 nm Mg doped GaN layer is grown to cap the structure succeeded by an anneal treatment in the growth reactor in a nitrogen atmosphere at 700 °C to activate the Mg dopant.

To allow structural characterization via scanning transmission electron microscopy (STEM), a cross-sectional lamellae was prepared by using a FEI Helios NanoLabTM focused ion beam (FIB) *in situ* lift-out method. A FIB voltage of 30 kV is used initially, followed by a 5 kV treatment to reduce ion damage. The specimen thickness is 95–120 nm, based on an electron energy loss spectroscopy (EELS) measurement.

An analytical TEM (FEI Tecnai Osiris) equipped with a four-energy dispersive x-ray spectroscopy (EDS)-detector SuperX system

FIG. 2. A schematic diagram of the sample structure.

is used for structural and compositional analysis at 200 kV. High-angle annular dark-field (HAADF) STEM images are taken with the beam direction parallel to the [1-10] zone axis. The correlation of alloy segregation and the exact position of the stacking faults are studied in an aberration-corrected STEM (FEI Titan 80–200[26]), operating voltage of 200 kV, equipped with a SuperX system and drift correction functionality. The beam convergence angle and the beam current used were 19 mrad and 100 pA for Osiris and 24.7 mrad and 582 pA for Titan 20–200. The annular dark-field detector semi-angle used was 69–200 mrad.

The EDS edges used are K_α peak for Ga (9.241 keV), L_α peak for In (3.286 keV), and K_α peak for Al (1.486 keV), respectively. In quantitative analysis, the EDS spectra are denoised by principle component analysis (PCA)[27] and the relative concentration of each element present is calculated with Cliff–Lorimer (CL) method.[28]

III. RESULTS

Cross-sectional STEM was used to characterize the correlation between SFs and local composition variations with sub-nanometre spatial resolution. Figure 3(a) shows an overview cross-sectional HAADF STEM image (zone axis = [1-10]) of the heterostructure. The planar (-1-11) and (111) SFs are visible as inclined lines of contrast running through the multilayer with some of them highlighted by red arrows. The density of SFs near the GaN/SiC interface is high but decreases rapidly to about 0.5×10^6 cm^{-1} within the first 100 nm, as a result of partial dislocation reactions or termination by a Shockley partial dislocation.[29] Individual SFs and

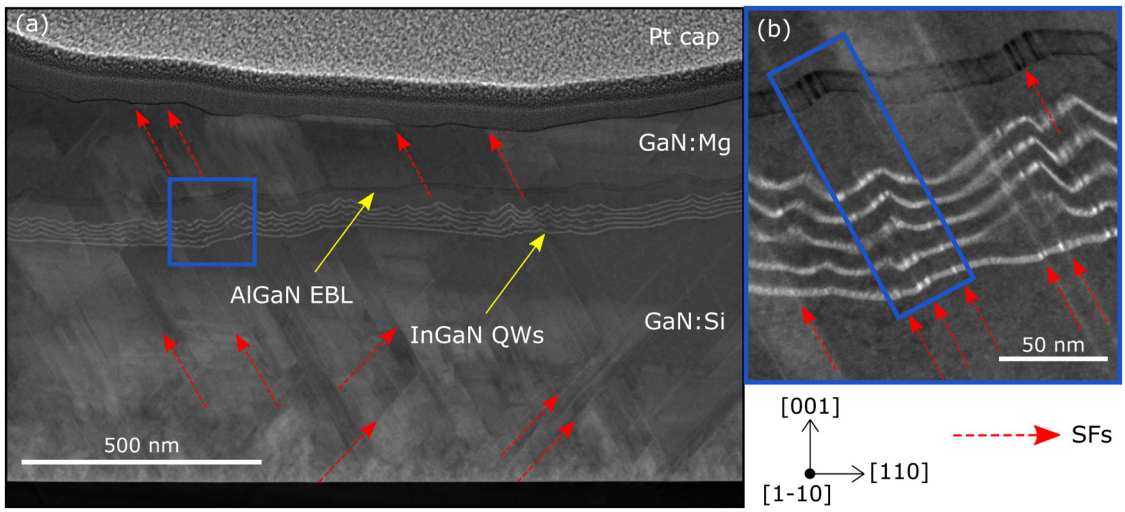

FIG. 3. (a) HAADF STEM image of an overview of the sample structure. (b) HAADF STEM image of the QW region highlighted by the blue rectangle in (a). The region enclosed by the blue rectangle in (b) is further analyzed by EDS. The red arrows show some example stacking faults in the sample. The region enclosed by the blue rectangle in (b) is further analyzed by EDS. The red arrows show some example stacking faults in the sample.

groups of planar defects tend to roughen the growth surface locally causing buckling of the InGaN QWs as observed in cross section. Figure 3(b) shows a higher magnification image of the area highlighted by the blue square in Fig 3(a), which contains both the five InGaN QWs (bright lines) and the AlGaN EBL (darker contrast) in the GaN matrix (gray). Changes in intensity are observed where the SFs intersect the InGaN and AlGaN layers. A change in the HAADF contrast generally indicates variations in composition, although the contrast changes could also be affected by crystallinity, local lamella thickness variation, and local strain. However, the HAADF contrast changes observed in Fig 3(b) suggests that, around the SFs, the alloy composition of both the QWs and the EBL are changing.

In order to examine the group-III elemental distribution in the vicinity of stacking faults, EDS mapping was used on the region marked by the blue rectangle in Fig. 3(b). The pixel size of the EDS mapping is 1.0 nm^2 and the average count of x rays at each pixel is 2502. Here, the relative compositions are given as group-III site fraction x for In, y for Al, and (1–x)/(1–y) for Ga, respectively, in $In_xGa_{1-x}N$ and $Al_yGa_{1-y}N$. All the site fractions were calculated from the STEM-EDS signal using CL factors and processed by the open source Python library HyperSpy.[30] Figure 4(a) is a Ga distribution map in the region marked in Fig. 3(b). Note that in Fig 4, the images are oriented such that the SFs run horizontally. The arrows highlight the approximate positions of SFs. Within the alloy layers, the Ga content drops sharply around the SFs. For comparison, in the GaN matrix and the GaN QBs, the Ga content remains close to unity, as expected. Figure 4(b) shows the In and Al distribution of the same region

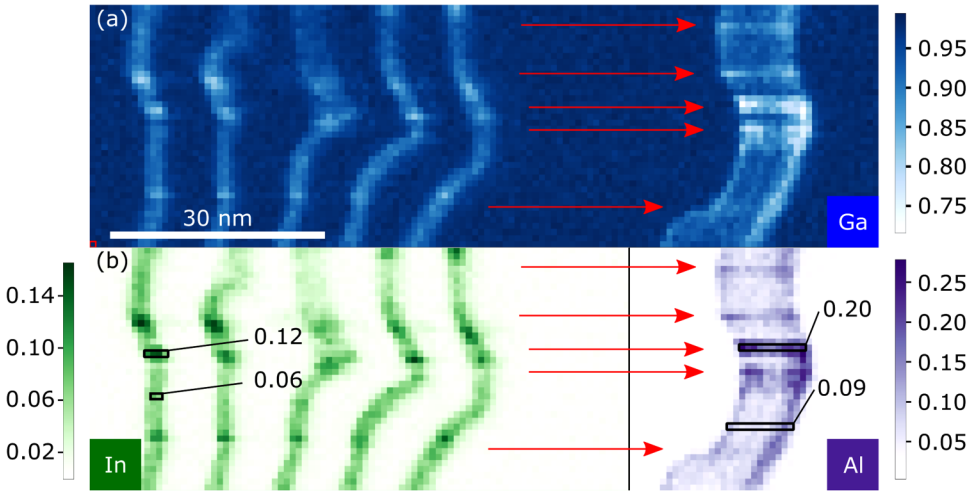

FIG. 4. (a) Group-III site fraction map of Ga and (b) Group-III site fraction of In and Al of the region marked in Fig. 3(b) measured by STEM-EDS. The red arrows indicate the approximate positions of relevant SFs. The black boxes highlight the exact group-III site fractions of In and Al at stacking faults and at undefected areas, respectively.

TABLE I. The averages of In and Al group-III site fractions at SFs and Far from SFs and the ration between them.

	Average Group-III site fraction		
Group-III element	Near SF (%)	Matrix (%)	Ratio (near SF/matrix)
In	15 ± 4	6.4 ± 2	2.3 ± 1.3
Al	15 ± 2	8.1 ± 1	1.9 ± 0.5

displayed in (a). The InGaN QWs are seen as green bands of varying intensity, whereas the AlGaN EBL is a purple band. Considering the material within the QW and the EBL, respectively, both the In content and the Al content show a dramatic increase near SFs compared to the adjacent material, as highlighted by the black boxes in Fig. 4(b), for which the relevant local compositions are labeled.

To quantify the local impact of the SFs on the alloy composition, ten regions of different SF locations were selected in both the QW and the EBL and compared to ten regions away from SFs. Their compositions are calculated from EDS data. The average values are given in Table I, as well as the ratio of Group-III element fractions near SF to those of the adjacent matrix. The In and Al content around SFs are approximately a factor of 2.3 and 1.9 higher, respectively, than the adjacent alloy material.

To pinpoint the locations of the In- and Al-enriched regions relative to the SFs, Fig. 5(a) shows a high-resolution HAADF STEM image of two InGaN QWs (zone axis = [1-10]). The red arrows mark the fault where the ABCABCABC stacking changes to ABC**AC**ABC, indicating the presence of a single, intrinsic stacking fault. A higher magnification image of the defected region at the top QW is displayed in the inset, and the yellow, green, and purple dots illustrate the stacking order of the (111) planes. EDS mapping was performed on the same region of the HAADF STEM image allowing direct localization of In-rich regions compared to the SFs. Figures 5(b) and 5(c) are the EDS peak intensity maps of the elements Ga and In, respectively. The pixel size of the EDS mapping is 0.39 nm^2 and the average count of x rays at each pixel is 97. To visualize the impact of the SFs, a line profile indicated by the yellow arrows and integrated over a width of 4 nm to increase the signal-to-noise ratio was taken at the top QW. The resulting average profiles from the HAADF, Ga and In maps are shown in Fig. 5(d). For each data point in the line scan, the average x-ray count within the Ga-K_α and In-L_α peaks are 147 and 41, respectively.

The location of the SF is identified by noting the HAADF contrast at the location of the SF in the image and matching the corresponding contrast change in the profile. Compared to the surrounding material, the intensity of the Ga signal is slightly reduced within a ~2 nm range on either side of the SF. The In signal intensity on the other hand increases significantly on either side of the SF resulting in two peaks each about 1.2–1.5 nm away from the SF. At the location of the SF itself, the In signal intensity reduces to a level similar to that in the surrounding material at some distance from the SF. The observations indicate that the higher In content associated with the SFs occurs adjacent to them and not directly on the defect.

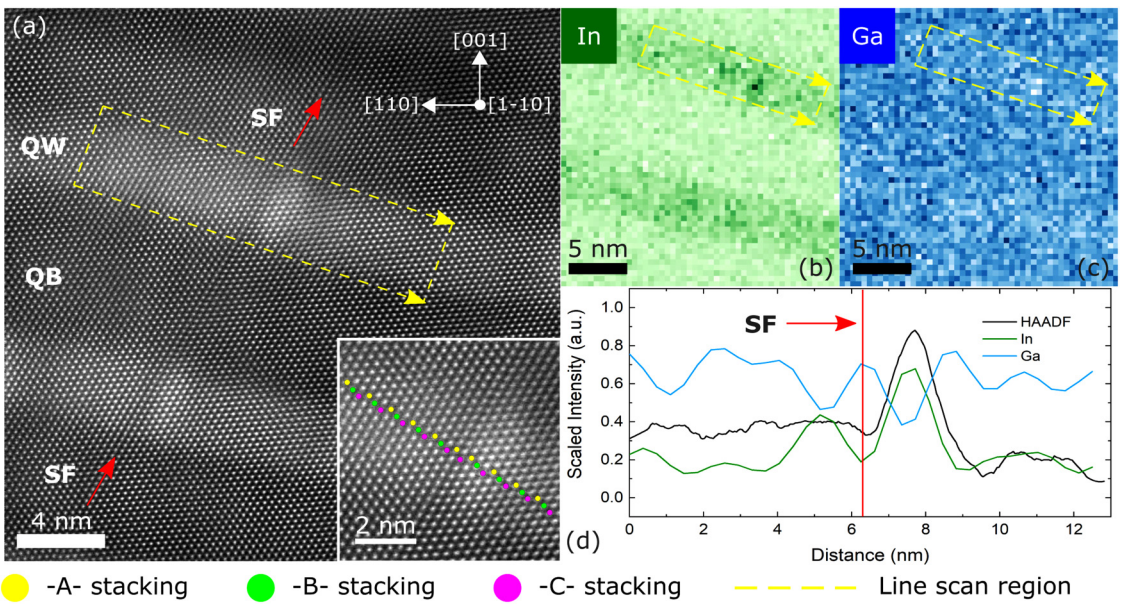

FIG. 5. (a) Shows the high-resolution HAADF STEM image of two InGaN QWs. The red arrows illustrate an intrinsic SF. The inset displays a magnified image of the top QW around the SF and the yellow, green, and purple dots indicate the atomic columns with stacking type of -A-, -B-, and -C-, respectively. (b) is the In EDS signal map corresponding to (a), and (c) is the Ga EDS signal map corresponding to (a). The yellow arrows in (a), (b), and (c) mark a line scan taken on the top QW. (d) shows the resulting average profiles from the line scan on (a)–(c).

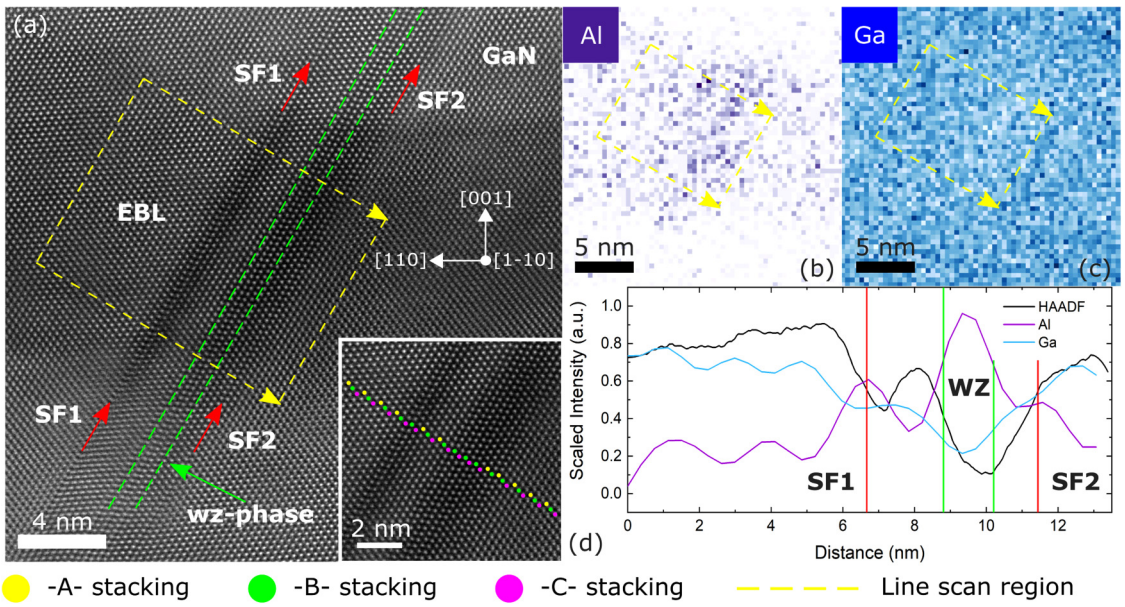

FIG. 6. (a) Shows the high-resolution HAADF STEM image of an EBL. The red arrows illustrate two intrinsic SFs, and the green lines enclose a small wurtzite inclusion. The inset displays a magnified image of the EBL around the defected area and the yellow, green, and purple dots indicate the atomic columns with stacking type of -A-, -B-, and -C-, respectively. (b) is the Al EDS signal map corresponding to (a), and (c) is the Ga EDS signal map corresponding to (a). The yellow arrows in (a)–(c) mark a wide line scan taken on the EBL. (d) shows the resulting average profiles from the line scan on (a)–(c).

An asymmetry in the segregation of In can be observed around the SF in both the In map and the profile. Similar asymmetry can also sometimes be observed in lower-magnification EDS maps but it is not yet clear whether this asymmetry is universal nor what its origin may be.

The same approach was used to study the AlGaN EBL. A region with multiple defects, which exhibited good compositional contrast, was selected for this study. Figure 6(a) shows a high-resolution HAADF STEM image of the EBL (zone axis = [1-10]). A higher magnification image of the defected region in the EBL is shown in the inset to demonstrate its atomic structure. The red arrows illustrate two intrinsic SFs, SF1 and SF2, which interrupt the zb stacking to AB**CB**CABC and BCA**BA**BCA, respectively. Between the two SFs is a region enclosed by the green lines, which may be identified from its stacking sequence as a 1 nm-wide inclusion with wz stacking. The SFs and the wz inclusion are only separated by 1–2 nm apart. Figures 6(b) and 6(c) are the EDS peak intensity maps of Ga and Al, respectively, both taken on the same region of Fig. 6(a). The pixel size of the EDS mapping is 0.38 nm^2 and the average count of x rays at each pixel is 72. Due to a lower x-ray fluorescence yield of Al than In,[31] the EDS peak intensity map of Al [Fig. 6(b)] is nosier than that of In [Fig. 5(b)]. Therefore, a wider line profile indicated by the yellow arrows, integrated over a width of 10 nm, was taken along the EBL to reduce the noise in Fig. 6(d). The resulting profiles of the HAADF, Ga and Al signals are shown in Fig. 6(d). For each data point in the line scan, the average x-ray count within the Ga-K_α and Al-K_α peaks are 295 and 38, respectively. Across the whole defective region, the intensity of the Ga signal is weaker than that in the adjacent zb matrix. Three peaks can be seen in the Al profile at the locations of both the SFs and the wz inclusion. On the defect sites, the Al signal intensity level is more than double the level seen in the adjacent material. However, the Al signal intensity is reduced in the short zb regions that separate the defects. These data suggest that, in contrast to the In segregation adjacent to the stacking faults, the segregation of Al occurs at the location of a SF.

Overall, five SFs in InGaN QW layer and four SFs in AlGaN EBL were analyzed by high-resolution STEM-EDS. Although some of these SFs were not well isolated, similar segregation patterns for In and Al have been observed consistently.

IV. DISCUSSION

Segregation of alloying elements around SFs in GaN-based materials has not been widely reported in the literature but it has been observed in materials such as brass alloys, where this phenomenon is referred to as Suzuki segregation.[32] In brass alloys, the SF energy decreases as the concentration of certain solute atoms at the SF location increases. In general, this Suzuki segregation is discussed in relation to phase stability.[33] If SFs in the face centered cubic (fcc) brass matrix are regarded as local regions of hexagonal close packed (hcp) structure, atoms energetically more stable in the hcp structure rather than in the fcc matrix are expected to segregate to the SFs. In the III-nitride material system, however, wz is the thermodynamically more stable structure for all of AlN, GaN, and InN and their alloys with wz-GaN having a formation energy

slightly lower than zb-GaN with a difference of about 10 meV/atom.[34] We would expect the material with the lowest formation energy in the hcp phase to preferentially segregate to SFs. There are several reports[35,36] on the energy difference between the zb and wz structures but few on the absolute energy values of the wz structure of the three alloys. It is, thus, difficult to state with any certainty whether the understanding of Suzuki segregation gained from other materials can explain our observations.

At 300 K, the c lattice parameter of bulk wz-GaN and the lattice parameter of bulk zb-GaN are about 5.186 and 4.506 Å, respectively.[15,37–39] The interplanar spacing $d_{(0001)}$ in bulk wz-GaN is, therefore, 2.593 Å, and the equivalent interplanar spacing $d_{(111)}$ in bulk zb-GaN is, therefore, 2.602 Å. Bulk zb-GaN has a larger interplanar spacing between the close packed planes than bulk wz-GaN. This may be related to the Coulombic interaction between third-nearest-neighbor Ga and N atoms in the wurtzite phase. SFs can be seen as very short-range wurtzite regions, and their equilibrium interplanar spacing may, thus, be smaller than the interplanar spacing in the undefected zincblende material. Therefore, SFs will be preferential sites for smaller atoms, which imply Al atoms in the case of the AlGaN EBL and Ga atoms in the case of the InGaN QWs. This variation in lattice spacing might account for our experimental observation. However, given the difference in lattice spacing would be of the order of a few picometers, experimental proof of a smaller local lattice plane spacing is extremely difficult to obtain. This segregation of the smaller atom to the region with a smaller plane spacing could also lead to a lowering of the stacking fault energy and could, thus, be considered a variation on Suzuki segregation whereby both the local strain energy and the equilibrium energy of the relevant bulk phases are taken into account.

Finally, it is worth considering what impact the observed segregation around stacking faults might have on the properties of an LED. Inhomogeneity in the QW composition will certainly lead to variations in the emission energy and will, hence, broaden the emission bands. We will comment in more detail elsewhere[40] about the detailed impact of the observed structures on photoluminescence. The emission from zb-InGaN QWs is found to be optically polarized up to 70% at room temperature and this has been suggested to be associated with indium-rich nanostructures formed in the QWs due to their intersection with SFs. In terms of the AlGaN EBL, it is less obvious how this might affect device performance but the presence of Al-depleted regions will locally lower the barrier to electron overflow from the active region.

V. CONCLUSIONS

SF induced alloy segregation has been observed in zb-GaN heterostructure. High-resolution STEM and EDS analysis shows that indium tends to segregate next to the SFs in the InGaN QW and aluminum tends to segregate directly on the SFs in the AlGaN EBL. The segregation happens on a microscopic scale of about 2 nm but the composition change is as large as a factor of 2. We hypothesize that the observed segregation may result in a reduction in the stacking fault energy, which could relate either to differences in the bulk energies of wz III-nitride alloys or to differences in interplanar spacing between faulted and non-faulted regions. The change in compositions of the heterostructure is expected to cause emission band broadening and increased electron overflow. Detailed optical effects of this segregation are reported in Ref. 40.

ACKNOWLEDGMENTS

We would like to acknowledge funding from BEIS Energy Entrepreneurs fund 6 for their support of Kubos Semiconductors Ltd. We also acknowledge the support of Engineering and Physical Sciences Research Consul (EPSRC) through Grant Nos. EP/M010589/1 and EP/R01146X/1. D. J. Wallis would like to acknowledge the support of EPSRC through Grant No. EP/N01202X/1.

DATA AVAILABILITY

The data that support the findings of this study are openly available in the University of Cambridge repository at https://doi.org/10.17863/CAM.52125.

REFERENCES

[1]M. R. Krames, O. B. Shchekin, R. Mueller-Mach, G. O. Mueller, L. Zhou, G. Harbers, and M. G. Craford, J. Disp. Technol. **3**, 160 (2007).
[2]T. Mukai, M. Yamada, and S. Nakamura, Jpn. J. Appl. Phys. **38**, 3976 (1999).
[3]H. Sugawara, M. Ishikawa, and G. Hatakoshi, Appl. Phys. Lett. **58**, 1010 (1991).
[4]H. Sugawara, K. Itaya, H. Nozaki, and G. Hatakoshi, Appl. Phys. Lett. **61**, 1775 (1992).
[5]M. Auf der Maur, A. Pecchia, G. Penazzi, W. Rodrigues, and A. Di Carlo, Phys. Rev. Lett. **116**, 027401 (2016).
[6]D. S. P. Tanner, P. Dawson, M. J. Kappers, R. A. Oliver, and S. Schulz, Phys. Rev. Appl. **13**, 044068 (2020).
[7]I. Gherasoiu, K. M. Yu, L. A. Reichertz, V. M. Kao, M. Hawkridge, J. W. Ager, and W. Walukiewicz, Phys. Status Solidi B **247**, 1747 (2010).
[8]D. R. Elsaesser, M. T. Durniak, A. S. Bross, and C. Wetzel, J. Appl. Phys. **122**, 115703 (2017).
[9]H. Liu, A. C. Frenkel, J. G. Kim, and R. M. Park, J. Appl. Phys. **74**, 6124 (1993).
[10]Y. Hiroyama and M. Tamura, Jpn. J. Appl. Phys. **37**, L630 (1998).
[11]M. Häberlen, J. W. Gerlach, B. Murphy, J. K. N. Lindner, and B. Stritzker, J. Cryst. Growth **312**, 762 (2010).
[12]S. V. Novikov, N. M. Stanton, R. P. Campion, R. D. Morris, H. L. Geen, C. T. Foxon, and A. J. Kent, Semicond. Sci. Technol. **23**, 015018 (2008).
[13]D. G. Pacheco-Salazar, S. F. Li, F. Cerdeira, E. A. Meneses, J. R. Leite, L. M. R. Scolfaro, D. J. As, and K. Lischka, J. Cryst. Growth **284**, 379 (2005).
[14]J. Wu, H. Yaguchi, H. Nagasawa, Y. Yamaguchi, K. Onabe, Y. Shiraki, and R. Ito, Jpn. J. Appl. Phys. **36**, 4241 (1997).
[15]M. Frentrup, L. Y. Lee, S. Sahonta, M. J. Kappers, F. Massabuau, P. Gupta, R. A. Oliver, C. J. Humphreys, and D. J. Wallis, J. Phys. D Appl. Phys. **50**, 433002 (2017).
[16]H. Vilchis, V. M. Sanchez-R, and A. Escobosa, Thin Solid Films **520**, 5191 (2012).
[17]Z. H. Feng, H. Yang, S. M. Zhang, L. H. Duan, H. Wang, and Y. T. Wang, J. Cryst. Growth **235**, 207 (2002).
[18]M. Moret, S. Ruffenach-Clur, N. Moreaud, O. Briot, J. Calas, and R. L. Aulombard, Phys. Status Solidi A **176**, 493 (1999).
[19]H. Okumura, K. Ohta, G. Feuillet, K. Balakrishnan, S. Chichibu, H. Hamaguchi, P. Hacke, and S. Yoshida, J. Cryst. Growth **178**, 113 (1997).
[20]T. Suzuki, H. Yaguchi, H. Okumura, Y. Ishida, and S. Yoshida, Jpn. J. Appl. Phys. **39**, L497 (2000).
[21]M. Kakuda, S. Kuboya, and K. Onabe, J. Cryst. Growth **323**, 91 (2011).
[22]Y. L. Casallas-Moreno, S. Gallardo-Hernández, F. Ruiz-Zepeda, B. M. Monroy, A. Hernández-Hernández, A. Herrera-Gómez, A. Escobosa-Echavarría, G. Santana, A. Ponce, and M. López-López, Appl. Surf. Sci. **353**, 588 (2015).
[23]L. Y. Lee, M. Frentrup, M. J. Kappers, R. A. Oliver, C. J. Humphreys, and D. J. Wallis, J. Appl. Phys. **124**, 105302 (2018).

[24]R. M. Kemper, P. Veit, C. Mietze, A. Dempewolf, T. Wecker, F. Bertram, J. Christen, J. K. N. Lindner, and D. J. As, Phys. Status Solidi C **12**, 469–472 (2015).
[25]S. A. Church, S. Hammersley, P. W. Mitchell, M. J. Kappers, L. Y. Lee, F. Massabuau, S. L. Sahonta, M. Frentrup, L. J. Shaw, D. J. Wallis, C. J. Humphreys, R. A. Oliver, D. J. Binks, and P. Dawson, J. Appl. Phys. **123**, 185705 (2018).
[26] Ernst Ruska-Centre for Microscopy and Spectroscopy with Electrons, J. Large-scale Res. Facil. **2**, A43 (2016).
[27]I. T. Jolliffe and J. Cadima, Phil. Trans. R. Soc. A. **374**, 20150202 (2016).
[28]G. Cliff and G. W. Lorimer, J. Microsc. **103**, 203 (1975).
[29]L. Y. Lee, M. Frentrup, P. Vacek, M. J. Kappers, D. J. Wallis, and R. A. Oliver, J. Appl. Phys. **125**, 105303 (2019).
[30]F. de la Peña, E. Prestat, V. Tonaas *et al.*, hyperspy/hyperspy: HyperSpy v1.5.2 (2019).
[31]J. H. Hubbell, P. N. Trehan, N. Singh, B. Chand, D. Mehta, M. L. Garg, R. R. Garg, S. Singh, and S. Puri, J. Phys. Chem. Ref. Data **23**, 339 (1994).
[32]H. Suzuki, J. Phys. Soc. Jpn. **17**, 322 (1962).
[33]Y. Koizumi, T. Nukaya, S. Suzuki, S. Kurosu, Y. Li, H. Matsumoto, K. Sato, Y. Tanaka, and A. Chiba, Acta Mater. **60**, 2901 (2012).
[34]Z. Z. Bandić, T. C. McGill, and Z. Ikonić, Phys. Rev. B **56**, 3564 (1997).
[35]J. Serrano, A. Rubio, E. Hernández, A. Muñoz, and A. Mujica, Phys. Rev. B **62**, 16612 (2000).
[36]S. Q. Wang and H. Q. Ye, Phys. Status Solidi B **240**, 45 (2003).
[37]P. Rinke, M. Winkelnkemper, A. Qteish, D. Bimberg, J. Neugebauer, and M. Scheffler, Phys. Rev. B **77**, 075202 (2008).
[38]A. L. Rosa and J. Neugebauer, Phys. Rev. B **73**, 205346 (2006).
[39]M. E. Levinshtein, S. L. Rumyantsev, and M. S. Shur, *Properties of Advanced Semiconductor Materials: GaN, AIN, InN, BN, SiC, SiGe* (John Wiley & Sons, Inc., New York, 2001).
[40]S. A. Church, B. Ding, P. W. Mitchell, M. J. Kappers, M. Frentrup, G. Kusch, S. M. Fairclough, D. J. Wallis, R. A. Oliver, and D. J. Binks, Appl. Phys. Lett. **117**, 032103 (2020).